



## Experimental investigation on the corrosion inhibition characteristics of mild steel by 5-(2-hydroxyphenyl)-1,3,4-oxadiazole-2-thiol in hydrochloric acid medium

H. Ouici <sup>a</sup>, M. Tourabi <sup>b</sup>, O. Benali <sup>c,\*</sup>, C. Selles <sup>d</sup>, M. Traisnel <sup>e</sup>, C. Jama <sup>e</sup>,  
F. Bentiss <sup>b,e</sup>, R. Salghi <sup>f</sup>

<sup>a</sup> Department of chemistry, Faculty of Sciences, Univesrity Dr Moulay Tahar, Saïda, Algeria

<sup>b</sup> Laboratoire de Catalyse et de Corrosion des Matériaux (LCCM), Faculté des Sciences, Université Chouaib Doukkali, B.P. 20, M-24000 El Jadida, Morocco

<sup>c</sup> Department of Biology, Faculty of Sciences, Univesrity Dr Moulay Tahar, Saïda, Algeria

<sup>d</sup> Department of chemistry, Faculty of Sciences, Univesrity of Tlemcen, Tlemcen, Algeria

<sup>e</sup> UMET-PSI, CNRS UMR 8207, ENSCL, Université Lille I, CS 90108, F-59652 Villeneuve d'Ascq Cedex, France

<sup>f</sup> Engineering Team of Environment and Biotechnology, ENSA, Ibn Zohr University, PO Box 1136, 80000 Agadir, Morocco

Received 17 Dec 2015, Revised 01 Jul 2016, Accepted 02 Jul 2016

\*Corresponding author. E-mail: Email: [benaliomar@hotmail.com](mailto:benaliomar@hotmail.com)

### Abstract

5-(2-Hydroxyphenyl)-1,3,4-oxadiazole-2-thiol (5-HOT) was studied as corrosion inhibitor for mild steel in 1 M HCl using different methods ( weight loss measurements and electrochemical techniques. The results showed that this compound is good corrosion inhibitor for studied system, and its inhibition efficiency increased with inhibitor concentration, reaching a maximum of 95 % with 0.5 mM of 5-HOT at 303 K. Potentiodynamic polarization study revealed that 5-HOT acts as mixed inhibitor and The ac impedance study showed that the double-layer capacitance decreased and charge-transfer resistance increased with increase in the inhibitor concentration, involving increased in inhibition efficiency. The influence of the temperature on the inhibitor efficiency was also studied. The adsorption of 5-HOT was well described by the Langmuir adsorption isotherm. Activation and the adsorption thermodynamic parameters were calculated and discussed. The chemical composition of the protective film was determined by X-Ray Photoelectron Spectroscopy (XPS).

**Keywords:** A. Mild steel; A. Acid solutions; B. XPS; B. EIS; C. Acid inhibition.

### 1. Introduction

Corrosion and corrosion inhibition of iron and iron alloys, in general, and steel, in particular, have received a great attention in different media [1–5] with and without various types of inhibitors. Steel, the most widely used in engineering material, accounts for approximately 85 % of the annual steel production worldwide [6]. The corrosion inhibition efficiency of organic compounds is related to their adsorption properties [7-8].

Up to now, many N-heterocyclic compounds are reported as good corrosion inhibitors for iron or steel in acidic media especially oxadiazole derivatives, such as 2,5-bis (3,4,5-trimethoxy phenyl)-1,3,4-oxadiazole [9], 4-(((4-((5-Mercapto-1,3,4-oxadiazol-2-yl)methyl)-5-methylthiazol-2-yl)imino)methyl)benz ene-1,2-diol [10], 4-(((4-((5-Mercapto-1,3,4-oxadiazol-2-yl)methyl)-5-methylthiazol-2-yl)imino)methyl)-2,6-dimethoxyphenol [10],-[1,2,4]-triazole-methyl-4-acetyl-5-nitrophenyl-[1,3,4]-oxadiazole [ 11], 1-phenyl-2-(5-(1,2,4) triazol-1-ylmethyl-(1,3,4) oxadizaol-2-ylsulphanyl)-ethanone [12], 2-(4-tert-butyl-benzylsulphanyl)-5- (1,2,4) triazol-1-ylmethyl-(1,3,4) oxadiazole [12 ], 3,5-bis(n-pyridyl)-1,2,4-oxadiazoles (n-DPOX) [13], 2,5-bis(4-methoxyphenyl)-1,3,4-oxadiazole [14], 2,5-Bis(4-dimethylaminophenyl)-1,3,4-oxadiazole [15] and 2,5-bis(4-dimethylamino-phenyl)-1,3,4-thiadiazole [15].

The present work was designed to study the corrosion inhibition of mild steel in 1 M HCl solutions by 5-(2-hydroxyphenyl)-1,3,4-oxadiazole-2-thiol (5-HOT) as corrosion inhibitor using weight loss, different electrochemical techniques and X-ray photoelectron spectroscopy (XPS).

## 2. Experimental details

### 2.1. Materials

The tested inhibitor, namely 5-(2-hydroxyphenyl)-1,3,4-oxadiazole-2-thiol (5-HOT), was synthesised according to a previously described experimental procedure [16-18]. The molecular structure of 5-HOT is shown in Fig. 1. Mild steel, composed of : C  $\leq$  0.1 %, Si  $\leq$  0.03 %, Mn  $\leq$  0.2 %, P  $\leq$  0.02 %, Cr  $\leq$  0.05 %, Ni  $\leq$  0.05 %, Al  $\leq$  0.03 %, and the remainder iron, was used as the working electrode for all studies. The acid solutions (1 M HCl) were prepared by dilution of an analytical reagent grade 37 % HCl with doubly distilled water.

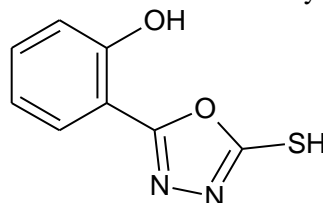


**Fig. 1.** Structure of 5-(2-hydroxyphenyl)-1,3,4-oxadiazole-2-thiol (5-HOT).

### 2.2. Weight loss method

For the weight loss measurements, the experiments were carried out in solution of 1 M HCl acid (uninhibited and inhibited) on mild steel sheets (15 mm  $\times$  15 mm  $\times$  2 mm). They were polished successively with different grades of emery paper up 1000 grade and each run was carried out in a glass vessel containing 100 ml of the test solution. A clean weight mild steel sample was completely immersed at an inclined position in the vessel. After 1 h of immersion in 1 M HCl with and without addition of inhibitor at different concentrations, the specimen was withdrawn, rinsed with distilled water, washed with ethanol, dried, and weighed.

### 2.3. Electrochemical measurements

Electrochemical measurements were performed in a conventional three-electrode cylindrical Pyrex glass cell. The temperature is thermostatically controlled at 303 K. Mild steel specimen was used as the working electrode, a platinum electrode as the counter electrode and a saturated calomel electrode (SCE) as the reference electrode. The working electrode (WE) in the form of disc cut from steel has a geometric area of 1 cm<sup>2</sup> and is embedded in polytetrafluoroethylene (PTFE). A fine Luggin capillary was placed close to the working electrode to minimize IR drop. All test solutions were de-aerated in the cell by using pure nitrogen for 10 min prior to the experiment. During each experiment, the test solution was mixed with a magnetic stirrer and the gas bubbling was maintained. Solartron Instruments SI 1287 potentiostat monitored by a personal computer via a GPIB Interface and CorrWare 2.80 software were used to run the tests and to collect the experimental data. Before each Tafel experiment, the mild steel electrode was pre-polarised at  $-800$  mV<sub>SCE</sub> for 10 min and thereafter the WE was allowed to corrode freely and its open circuit potential (OCP) was recorded as a function of time up to 1 h, the time necessary to reach a quasi-stationary value for the open-circuit potential. This steady-state OCP corresponds to the corrosion potential ( $E_{\text{corr}}$ ) of the WE.

Ac impedance measurements were performed using a potentiostat Solartron SI 1287 and a Solartron 1255B frequency response analyzer and ZPlot 2.80 software was used to run the tests and to collect the experimental data. The response of the electrochemical system to ac excitation with a frequency ranging from 10<sup>5</sup> Hz to 10<sup>-1</sup> Hz and peak to peak amplitude of 10 mV was measured with data density of 10 points per decade. All EIS diagrams were recorded at the open circuit potential, i.e., at the corrosion potential  $E_{\text{corr}}$ . One EIS spectrum is recorded usually within 10 min. The impedance data were analysed and fitted with the simulation ZView 2.80, equivalent circuit software.

For linear polarization resistance (LPR) measurements, the WE was polarised only in the range  $\pm 10$  mV vs.  $E_{\text{corr}}$  at a scan rate of 0.167 mV s<sup>-1</sup>. After studying ac impedance and LPR tests, the potentiodynamic Tafel measurements were scanned from cathodic to the anodic direction,  $E = E_{\text{corr}} \pm 200$  mV, with a scan rate of 0.5 mV s<sup>-1</sup>. The Tafel and LRP data were analysed and fitted using the polarization CorrView 2.80 software (Scribner Associates, Inc.).

### 2.4. X-ray photoelectron spectroscopy (XPS)

X-ray photoelectron spectroscopy (XPS) spectra were recorded by a XPS KRATOS, AXIS Ultra<sup>DLD</sup> spectrometer with the monochromatized Al-K $\alpha$  X-ray source ( $h\nu = 1486.6$  eV) and an X-ray beam of around 1mm. The analyser was operated in constant pass energy of 40 eV using an analysis area of approximately 700  $\mu\text{m} \times 300 \mu\text{m}$ . Charge compensation was applied to compensate for the charging effects that occurred during the

analysis. The C1s (285.0 eV) binding energy (BE) was used as internal reference. The spectrometer BE scale was initially calibrated against the Ag 3d<sub>5/2</sub> (368.2 eV) level. Pressure was in the 10<sup>-10</sup> torr range during the experiments. Quantification and simulation of the experimental photopeaks were carried out using CasaXPS software. Quantification took into account a non-linear Shirley background subtraction [19]. The disk mild steel (1 cm<sup>2</sup>) was pre-treated by the same procedure as for the gravimetric test. After 6 h of immersion at 303 K, the mild steel sheet was rinsed with acetone and ultra pure water.

### 3. Results and discussion

#### 3.1. Corrosion inhibition evaluation

##### 3.1.1. Weight loss studies

Table 1 gives the corrosion rate ( $W_{\text{corr}}$ ) and inhibition corrosion efficiency ( $\eta_{\text{WL}}$ ) obtained by conducting weight loss measurements for mild steel in the absence and presence of different concentrations of 5-(2-hydroxyphenyl)-1,3,4-oxadiazole-2-thiol (5-HOT) in 1 M HCl after 1 h of immersion in the different temperatures (303-333 K) and the inhibition efficiency (%) was determined by using the following equation:

$$\eta_{\text{WL}} (\%) = \left( 1 - \frac{w_i}{w_0} \right) \times 100 \quad (1)$$

where  $w_0$  and  $w_i$  are the values of corrosion weight losses of mild steel in uninhibited and inhibited solutions, respectively.

Analysing the obtained results in Table 1 reveals that  $\eta_{\text{WL}}$  (%) of mild steel increases with the increase of 5-HOT concentration up to 95% at 303 K and as the temperature increases, the inhibition efficiency decreases. It should be noted that, at 313, 323 and 333 K maximum inhibition efficiencies of 90.85, 88.53 and 84.37 % were obtained in studied system and the increase in corrosion rate is more pronounced with the rise of temperature for the uninhibited acid solution. The presence of inhibitor leads to decrease of the corrosion rate.

**Table 1.** Corrosion parameters obtained from weight loss for mild steel in 1 M HCl containing various concentrations of 5-HOT at different temperatures.

Temperature (K)	Concentration (mM)	$W_{\text{corr}}$ (mg cm <sup>-2</sup> h <sup>-1</sup> )	$\eta_{\text{WL}}$ (%)
303	Blank	4.20	—
	0.1	1.32	68.57
	0.2	1.05	75.00
	0.3	0.60	85.70
	0.4	0.44	89.50
	0.5	0.21	95.00
313	Blank	4.70	—
	0.1	1.75	62.76
	0.2	1.32	71.91
	0.3	0.81	82.76
	0.4	0.77	83.60
	0.5	0.43	90.85
323	Blank	8.20	—
	0.1	4.22	48.53
	0.2	2.73	66.70
	0.3	2.13	74.02
	0.4	1.47	82.07
	0.5	0.94	88.53
333	Blank	14.14	—
	0.1	7.30	48.37
	0.2	6.59	53.39
	0.3	4.22	70.14
	0.4	3.60	74.54
	0.5	2.21	84.37

The corrosion inhibition tests at different immersion times were also carried out on mild steel under similar conditions using the optimal concentration of the inhibitor (Fig. 2). From this figure, we can see that the inhibition efficiency of 5-HOT increased with immersion time. The increase in the inhibition efficiency may be due to the adsorption of 5-HOT to form an adherent film on the metal surface and suggests that the coverage of the metal surface with this film decreases the double layer thickness.

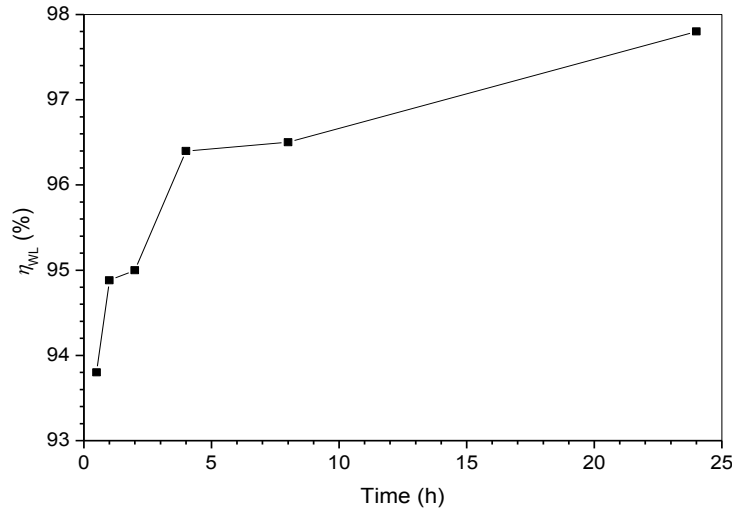


**Fig. 2.** Variation of inhibition efficiency with immersion time for M-steel in the presence 5-HOT at 303 K.

### 3.1.2. Polarization curves

Fig. 3 presents the potentiodynamic polarization curves for mild steel in 1 M HCl in the absence and presence of different concentrations of 5-HOT at 303 K and 1h of immersion. Values of associated electrochemical parameters such as corrosion potential ( $E_{corr}$ ), corrosion current density ( $I_{corr}$ ), cathodic Tafel slope ( $\beta_c$ ) and the calculated  $\eta_{Tafel} (%)$  are presented in Table 1. In this case, the inhibition efficiency is defined as follows:

$$\eta_{Tafel} (%) = \frac{I_{corr} - I_{corr(i)}}{I_{corr}} \times 100 \quad (2)$$

where  $I_{corr}$  and  $I_{corr(i)}$  are the corrosion current densities for steel electrode in the uninhibited and inhibited solutions, respectively, determined by extrapolation of cathodic Tafel lines to the corrosion potential.

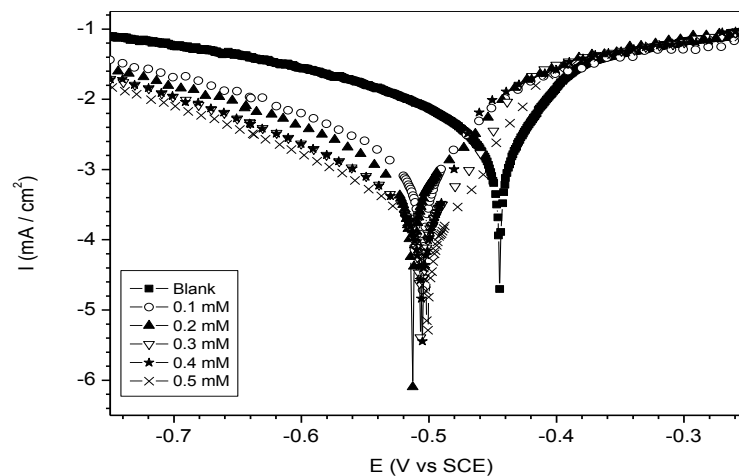


**Fig. 3.** Potentiodynamic polarization curves for M-steel in 1 M HCl containing different concentrations of 5-HOT at 303 K.

From Fig. 3, in the cathodic domain, it is clear that the cathodic current density decreases with increasing the concentration of the inhibitor; this indicates that these compounds are adsorbed on the metal surface and hence inhibition occurs. The values of  $b_c$  changed with increasing inhibitor concentration, which

indicates the influence of the compound on the kinetics of hydrogen evolution. The presence of 5-HOT displaces  $E_{\text{corr}}$  towards more negative potentials; this displacement in  $E_{\text{corr}}$  is  $< 85$  mV. This result shows that 5-HOT influences both cathodic and anodic branches. This implies that the inhibitor, 5-HOT, acts as a mixed-type inhibitor, affecting both anodic and cathodic reactions [19-22].

For anodic polarisation curves, it seems that the working electrode potential is higher than  $-380$  mV/SCE, the presence of the inhibitor does not change the current versus potential characteristics, this potential can be defined as desorption potential [23]. The phenomenon may be due to the obvious metal dissolution, leading to a desorption of the inhibitor molecules from the electrode surface, in this case the desorption rate of the inhibitors is higher than its adsorption rate, so the corrosion current increases more obviously with rising potential [24]. As it can be seen from these polarization results, the  $I_{\text{corr}}$  values decrease considerably in the presence of 5-HOT and decreased with increasing inhibitor concentration, and we notice that the inhibition efficiency increased with inhibitor concentration reaching a maximum value of 92.45% at 0.5 mM.

**Table 2.** Polarization data of mild steel in 1 M HCl containing different concentration of 5-HOT at 303 K.

Concentration (mM)	$-E_{\text{corr}}$ (mV vs SCE)	$-\beta_c$ (mV dec <sup>-1</sup> )	$I_{\text{corr}}$ ( $\mu\text{A cm}^{-2}$ )	$R_p$ ( $\Omega \text{ cm}^2$ )	$\eta_{\text{Tafel}}$ (%)	$\eta_{\text{LPR}}$ (%)
Blank	445.5	185	4.24	6.87	—	—
0.1	505.8	161	1.59	18.17	<b>62.5</b>	<b>62.19</b>
0.2	512.7	154	1.10	19.94	<b>74.05</b>	<b>65.55</b>
0.3	506.7	141	0.51	42.59	<b>87.97</b>	<b>83.87</b>
0.4	505.8	140	0.50	70.66	<b>88.21</b>	<b>90.27</b>
0.5	501.8	137	0.32	74.58	<b>92.45</b>	<b>90.79</b>

Linear polarisation resistance (LPR) technique was also performed in 1 M HCl with various concentrations of 5-HOT. The corresponding polarisation resistance ( $R_p$ ) values of mild steel in the absence and in the presence of different concentrations are given in Table 2. The inhibition percentage,  $\eta_{\text{LPR}}(\%)$ , calculated from  $R_p$  values are also presented in this Table. The increase in the  $R_p$  value suggests that the inhibition efficiency increases with the increase in the inhibitor concentration.

The inhibition efficiency of corrosion of mild steel is calculated by  $R_p$  as follows:

$$\eta_{\text{LPR}}(\%) = \frac{R_{p(i)} - R_p}{R_{p(i)}} \times 100 \quad (3)$$

where  $R_p$  and  $R_{p(i)}$  are the polarization resistance of mild steel electrode in the uninhibited and inhibited solutions, respectively.

### 3.1.3. Electrochemical impedance spectroscopy (EIS)

The effect of the 5-HOT on the corrosion behaviour of mild steel in 1 M HCl was also studied by ac impedance method at 303 K. Fig. 4 shows the Nyquist and Bode diagrams obtained at the open-circuit potential in 1 M HCl solution in the absence and presence of different concentrations of the inhibitor. Compared to uninhibited solution (blank), the size of the impedance diagram increases as the concentration rises and therefore the protection efficiency increases, which is an indication of the inhibition of the corrosion process. The Nyquist plots for all systems, in Fig. 4, generally have the form of only one depressed semicircle (capacitive loop) with one capacitive time constant as illustrated in Bode plots. The shape of the capacitive loops suggests that the corrosion process was mainly charge transfer controlled [25]. The general shape of the curves is very similar for all cases, indicating that no change occurs in the corrosion mechanism after inhibitor addition [26]. The impedance spectra were fitted by a simple Randles circuit, given in Fig. 5, which consists of  $R_s$  solution resistance,  $R_{ct}$  charge transfer resistance and CPE constant phase elements for the double layer. A constant phase element (CPE) is used instead of a pure capacitor to compensate for non-ideal capacitive response of the interface and to get a more accurate fit of experimental data set. Its impedance is given by Eq. (4):

$$Z_{\text{CPE}} = A^{-1} (i\omega)^{-n} \quad (4)$$

where  $A$  is proportionality coefficient (in  $\Omega^{-1} \text{ s}^n \text{ cm}^{-2}$ ),  $\omega$  is the angular frequency and  $i$  is the imaginary number,  $n$  is an exponent related to the phase shift and can be used as a measure of surface irregularity. For ideal electrodes, the CPE is equal to an ideal capacitor when  $n = 1$ .

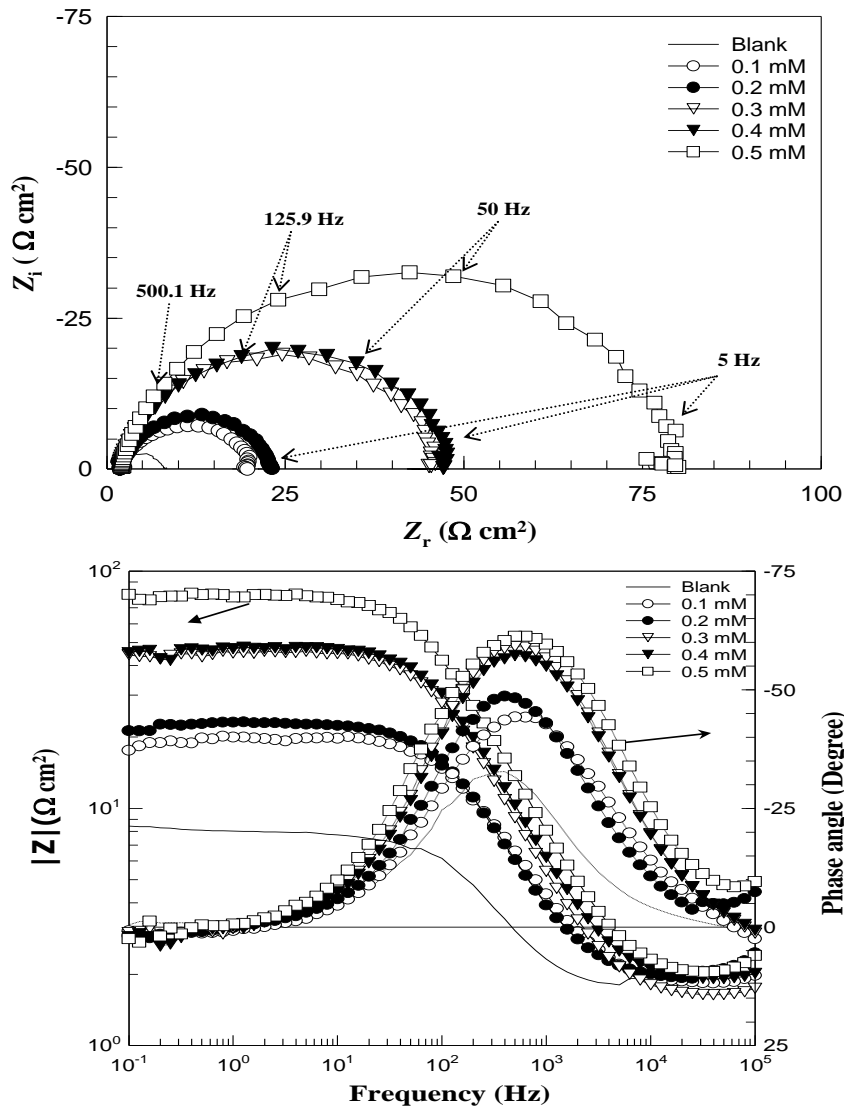


**Fig. 4.** Nyquist and Bode plots in absence and presence of different concentrations of 5-HOT in 1 M HCl.

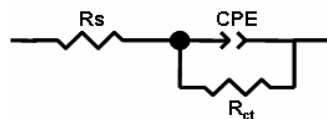


**Fig. 5.** Electrical equivalent circuit used for modeling the interface mild steel/1 M HCl solution without and with 5-HOT.

Simulation of Nyquist and Bode plots with above model is very close to the experimental data (Fig. 6, representative example). The fitting impedance parameters are given in Table 3. In the same table are shown also the calculated “double layer capacitance” values ( $C_{dl}$ ), using the Hsu and Mansfeld formula [27]:

$$C_{dl} = (AR_{ct}^{1-n})^{1/n} \quad (5)$$

and the relaxation time constant ( $\tau$ ) of charge-transfer process using the Eq. 6 [28]:

$$\tau = C_{dl} R_{ct} \quad (6)$$

The inhibition efficiency in the case of ac impedance study,  $\eta_z(\%)$ , was evaluated by  $R_{ct}$  values using Eq. 7, where  $R_{ct}$  and  $R_{ct(i)}$  were the charge transfer resistance of mild steel electrode in the absence and the presence of the inhibitor, respectively.

$$\eta_z(\%) = \frac{R_{ct(i)} - R_{ct}}{R_{ct(i)}} \times 100 \quad (7)$$

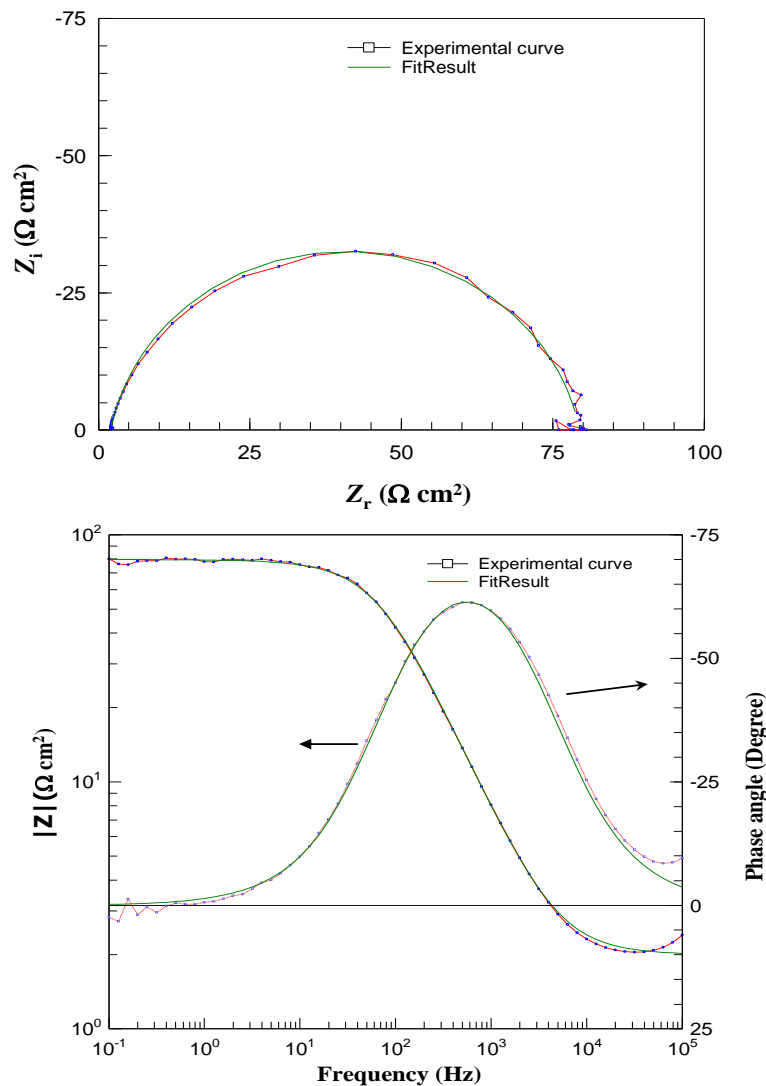


**Fig. 6.** EIS Nyquist and Bode diagrams for mild steel / 1 M HCl + 0.5 mM of 5-HOT interface: (···) experimental; (—) fitted data.

The inspection of the impedance results, given in Table 3, clearly shows that in the whole concentration range the increase of concentration 5-HOT increases the values of  $R_{ct}$ , indicating amelioration of the inhibitive properties. This effect is connected with diminishing of the  $C_{dl}$  value, often observed when adsorption of organic molecules on electrode surfaces takes place [29]. However, the values of the phase shift ( $n$ ) remains almost constant after addition of 5-HOT in the corrosive medium, indicating therefore that the charge transfer controlled dissolution mechanism of mild steel in 1 M HCl without and with inhibitor. The value of the proportional factor  $Q$  of the  $Z_{CPE}$  also varies in a regular manner with inhibitor concentration (Table 3). Also, the addition of 5-HOT to the corrosive solution increases the time constant ( $\tau$ ) value as well as the  $C_{dl}$  value decreases (Table 3), signifying that the charge and discharge rates to the metal-solution interface is greatly decreased. This shows that there is agreement between the amount of charge that can be stored (i.e. capacitance) and the discharge velocity in the interface ( $\tau$ ) [30]. Therefore, the double layer between the charged metal surface and the solution is considered as an electrical capacitor. Then, the adsorption of 5-HOT molecules on the mild steel surface decreases its electrical capacity because they displace the water molecules and other ions originally adsorbed on the surface. The decrease in this capacity with increase in 5-HOT concentration may be attributed to the formation of a protective layer on the electrode surface [31]. The thickness of this protective layer increases with increase in concentration, since more 5-HOT molecules will electrostatically adsorb on the electrode surface, resulting in a noticeable decrease in  $C_{dl}$ . This trend is in accordance with Helmholtz model, given by the following equation [32]:

$$C_{dl} = \frac{\epsilon \epsilon_0}{d} \quad (8)$$

where  $d$  is the thickness of the protective layer,  $\epsilon$  is the dielectric constant of the protective layer and  $\epsilon_0$  is the permittivity of free space ( $8.854 \times 10^{-14} \text{ F cm}^{-1}$ ).

The surface coverage ( $\theta$ ) can be estimated using from the inhibitor efficiency as  $\theta = \eta_z(\%) / 100$ . The linear decrease of  $C_{dl}$  with surface coverage  $\theta$ , given in Fig. 7, means that the capacitance contribution from the inhibitor-covered surface is solely due to the flat-adsorbed molecules at low surface coverage [33]. The ac impedance results also shows that the  $\eta_z(\%)$  increases continuously with increasing of the 5-HOT concentration and the maximum of 92.06 % was achieved in the case of 0.5 mM. The inhibition efficiencies, calculated from ac impedance study, show the same trend as these obtained from weight loss and polarization measurements. Therefore, these results suggest, once again, that this oxadiazole derivative (5-HOT) could serve as an effective corrosion inhibitor.

**Table 3.** Impedance data of mild steel in absence and presence of different concentrations of 5-HOT at 303 K.

Concentration (mM)	$R_s$ ( $\Omega \text{ cm}^2$ )	$R_{ct}$ ( $\Omega \text{ cm}^2$ )	$n$	$Q \times 10^4$ ( $\text{s}^n \Omega^{-1} \text{ cm}^{-2}$ )	$C_{dl}$ ( $\mu\text{F cm}^{-2}$ )	$T$ (s)	$\eta_z$ (%)
Blank	1.69	6.25	0.86	47.56	184.3	0.0011	—
0.1	1.789	18.50	0.85	1.88	63.6	0.0012	66.21
0.2	1.908	21.15	0.85	1.55	51.7	0.0012	70.45
0.3	1.608	44.59	0.88	0.87	40.4	0.0018	85.98
0.4	1.873	46.41	0.88	0.83	37.7	0.0018	86.53
0.5	1.881	78.69	0.87	0.69	30.8	0.0024	92.06

### 3.2. Effect of temperature

#### 3.2.1. Thermodynamic adsorption parameters

The nature of corrosion inhibition has been deduced in terms of the adsorption characteristics of the inhibitor. Metal surface in aqueous solution is always covered with adsorbed water dipoles. Therefore, adsorption of inhibitor molecules from aqueous solution is a quasi substitution process. A correlation between surface coverage ( $\theta$ ), defined by  $\eta(\%) / 100$ , and the concentration of inhibitor ( $C_{inh}$ ) in electrolyte can be represented by the Langmuir adsorption isotherm:

$$\frac{C_{inh}}{\theta} = \frac{1}{K_{ads}} + C_{inh} \quad (5)$$

where  $C_{inh}$  is the concentration of inhibitor and  $K_{ads}$  the adsorptive equilibrium constant.

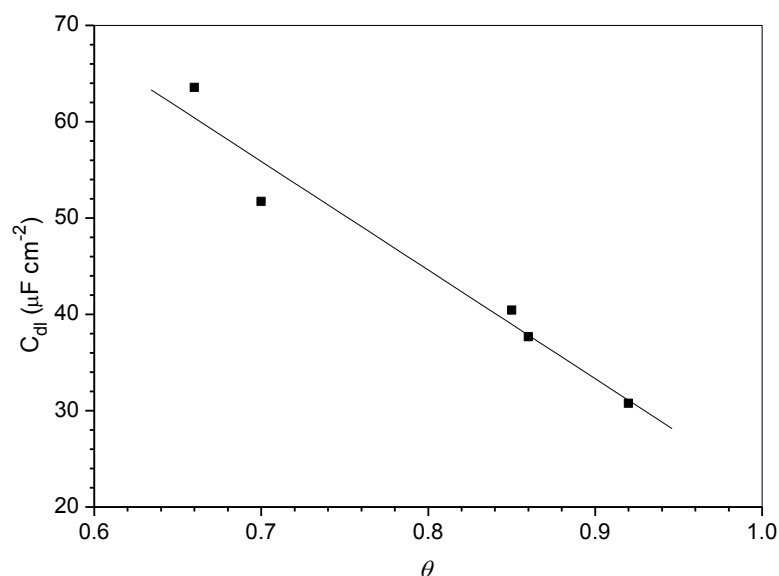


**Fig. 7.** The double-layer capacitance as function of the surface coverage.

Surface coverage values ( $\theta$ ) for the inhibitor were obtained from the weight loss measurements for various concentrations at different temperatures (303–333 K), as shown in Table 1. The best fitted straight lines were obtained for the plot of  $C_{inh}/\theta$  versus  $C_{inh}$  with slopes around unity. The correlation coefficient ( $R^2$ ) was used to choose the isotherm that best fit experimental data. This suggests that the adsorption of 5-HOT on metal surface followed the Langmuir adsorption isotherm (Fig. 8).

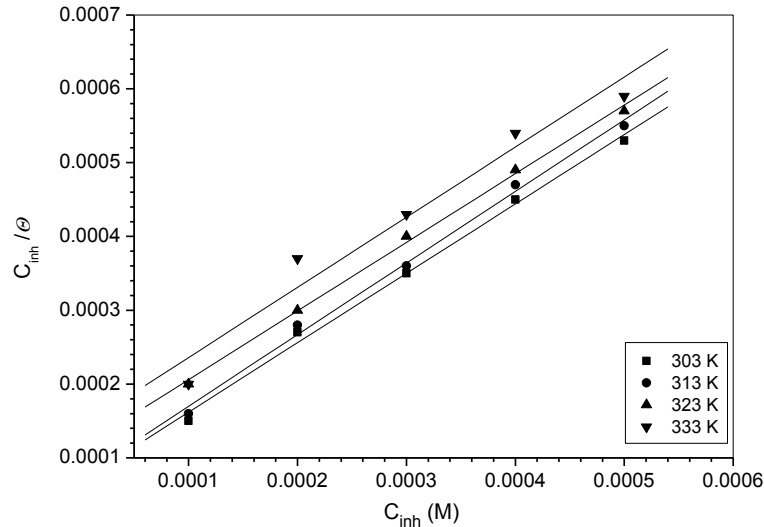


**Fig. 8.** Langmuir's isotherm adsorption model of 5-HOT on the mild steel surface in 1 M HCl at different temperatures.

Moreover, the essential characteristic Langmuir isotherm can be expressed in terms of a dimensionless separation factor,  $R_L$ , which describes the type of isotherm and is defined by [34-36]:

$$R_L = \frac{1}{1 + (K_{ads} \times C_{inh})} \quad (6)$$

The smaller  $R_L$  value indicates a highly favorable adsorption. If  $R_L > 1$ , unfavorable and  $0 < R_L < 1$ , favorable. Table 4 gives the estimated values of  $R_L$  for 5-HOT in 1 M HCl at different temperature. It was found that all  $R_L$  values are less than unity, confirming that the adsorption is favorable.

**Table 4.** Dimensionless separation factor  $R_L$  for 5-HOT at various temperatures

Conc. (mM)	Dimensionless separation factor ( $R_L$ )			
	303 K	313 K	323 K	333 K
0.1	0.40	0.42	0.53	0.58
0.2	0.25	0.27	0.36	0.41
0.3	0.18	0.20	0.27	0.32
0.4	0.14	0.15	0.22	0.26
0.5	0.12	0.13	0.18	0.22

From the intercepts of the straight lines  $C_{inh}/\theta$ -axis,  $K_{ads}$  values were calculated and are given in Table 5. The most important thermodynamic adsorption parameters are the free energy of adsorption ( $\Delta G_{ads}^{\circ}$ ), the heat of adsorption ( $\Delta H_{ads}^{\circ}$ ) and the entropy of adsorption ( $\Delta S_{ads}^{\circ}$ ). The adsorption constant,  $K_{ads}$ , is related to the standard free energy of adsorption,  $\Delta G_{ads}^{\circ}$ , with the following equation:

$$K_{ads} = \frac{1}{55.55} \exp\left(\frac{-\Delta G_{ads}^{\circ}}{RT}\right) \quad (7)$$

where  $R$  is the universal gas constant and  $T$  is the absolute temperature. The value 55.55 in the above equation is the concentration of water in solution in mol/l. The standard free energy of adsorption ( $\Delta G_{ads}^{\circ}$ ) values were calculated and given in Table 5. The negative values of  $\Delta G_{ads}^{\circ}$  indicate the stability of the adsorbed layer on the steel surface and spontaneity of the adsorption process. The increase of  $\Delta G_{ads}^{\circ}$  with temperature reveals that the inhibition of mild steel by 5-HOT is an exothermic process. In an exothermic process adsorption was

unfavourable with increasing reaction temperature due to the inhibitor desorption from the steel surface [37,38]. On the other hand, temperature increase is known to accelerate chemisorption on the inhibitor on the metal surface. If in a series of experiments the temperature increase causes an inhibition efficiency increase, especially when the  $\Delta G_{\text{ads}}^{\circ}$  diminishes reaching values higher than  $-40 \text{ kJ mol}^{-1}$ , the inhibitor adsorption is recognized as a chemisorption, involving an out-and-out sharing or transfer of electrons [39]. This really did not happen for the 5-HOT and found  $\Delta G_{\text{ads}}^{\circ}$  values were not lower than  $-40 \text{ kJ mol}^{-1}$ , but not higher than  $-34 \text{ kJ mol}^{-1}$ . It can be argued that 5-HOT adsorption mechanism in the temperature range of 303-333 K is ranging between a physisorption and chemisorption. The thermodynamic parameters  $\Delta H_{\text{ads}}^{\circ}$  and  $\Delta S_{\text{ads}}^{\circ}$  for the adsorption of 5-HOT on mild steel can be calculated from the following equation:

$$\Delta G_{\text{ads}}^{\circ} = \Delta H_{\text{ads}}^{\circ} - T \Delta S_{\text{ads}}^{\circ} \quad (8)$$

where  $\Delta H_{\text{ads}}^{\circ}$  and  $\Delta S_{\text{ads}}^{\circ}$  are the variation of enthalpy and entropy of the adsorption process, respectively. Fig. 9 shows the dependence of  $\Delta G_{\text{ads}}^{\circ}$  on T which indicates an appropriate relationship between thermodynamic parameters. The calculated values are given in Table 5.

**Table 5** Thermodynamic parameters for the adsorption of 5-HOT in 1 M HCl on the mild steel at different temperatures.

Temperature (K)	$K_{\text{ads}}$ (L/mol)	Slope	$R^2$	$\Delta G_{\text{ads}}^{\circ}$ (kJ mol <sup>-1</sup> )	$\Delta H_{\text{ads}}^{\circ}$ (kJ mol <sup>-1</sup> )	$\Delta S_{\text{ads}}^{\circ}$ (J mol <sup>-1</sup> K <sup>-1</sup> )
303	$1.47 \times 10^4$	0.98	0.994	-34.17	-19.23	49.4
313	$1.37 \times 10^4$	1.04	0.996	-34.74		
323	$0.88 \times 10^4$	0.96	0.998	-35.18		
333	$0.71 \times 10^4$	1.05	0.976	-35.67		

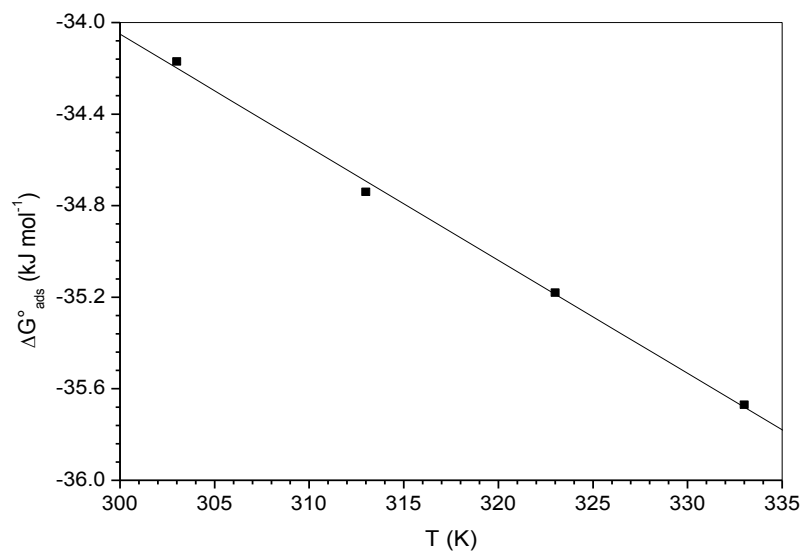


**Fig. 9.** Dependence of  $\Delta G_{\text{ads}}^{\circ}$  on T for mild steel in 1 M HCl containing 5-HOT.

Adsorption is an exothermic phenomenon ( $\Delta H_{\text{ads}}^{\circ} < 0$ ): the value obtained for the 5-HOT adsorption,  $-19.23 \text{ kJ mol}^{-1}$ , well agreed with this statement [40]. In aqueous solutions, the model of adsorption of organic molecules is generally accompanied by the desorption of water molecules, since the adsorption of an organic adsorbate at the metal-solution interface is considered a substitutional adsorption phenomenon [40]. Therefore, the adsorption of organic molecules is generally an exothermic phenomenon accompanied by a decrease in entropy; the contrary occurs for the desorption of the water molecules. The  $\Delta S_{\text{ads}}^{\circ}$  value obtained for the 5-HOT adsorption ( $49.4 \text{ J/mol K}$ ) is the algebraic sum of both contributions of the organic molecules adsorption and water molecules desorption [41]. Therefore, the positive  $\Delta S_{\text{ads}}^{\circ}$  value, related to substitutional adsorption, can be

attributed more to the increase of adsorbed inhibitor molecules rather than the decrease of water molecule desorption.

$\Delta H_{\text{ads}}^{\circ}$  and  $\Delta S_{\text{ads}}^{\circ}$  for the adsorption of 5-HOT on steel surface can be also deduced according to the Van't Hoff equation.

$$\text{Ln}K_{\text{ads}} = -\frac{\Delta H_{\text{ads}}^{\circ}}{RT} + \text{constant} \quad (9)$$

Fig. 10 shows the plot of  $\text{Ln} K_{\text{ads}}$  versus  $1/T$  which gives straight line with slope of  $\Delta H_{\text{ads}}^{\circ} / R$  and the intercept of  $(\Delta S_{\text{ads}}^{\circ} / R - \text{Ln}55.5)$ .

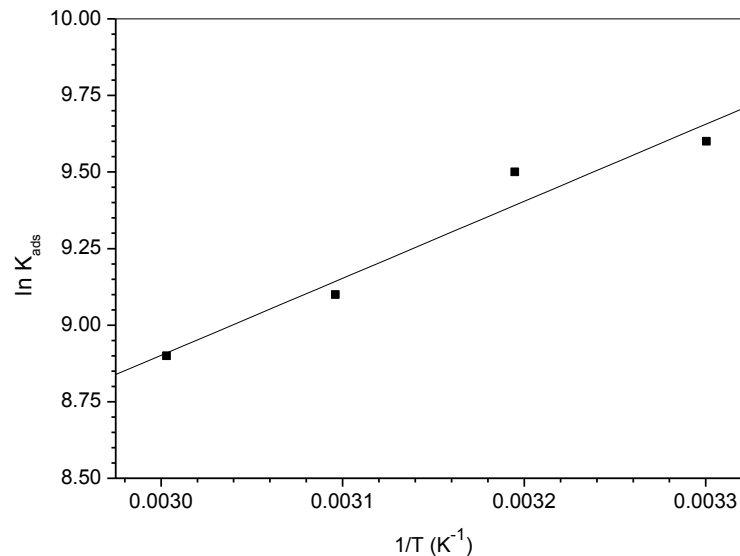


**Fig. 10.** Vant't Hoff plot for the mild steel/5-HOT/1 M HCl system.

The calculated  $\Delta H_{\text{ads}}^{\circ}$  using the Van't Hoff equation is  $-20.9 \text{ kJ mol}^{-1}$ , confirming the exothermic behaviour of the adsorption of 5-HOT on the steel surface. Values of  $\Delta H_{\text{ads}}^{\circ}$  obtained by the both method are in good agreement. Moreover, the deduced  $\Delta S_{\text{ads}}^{\circ}$  value of  $44.61 \text{ Jmol}^{-1}\text{K}^{-1}$  is very close to that obtained using the Eq. 8.

### 3.2.2. Thermodynamic activation parameters

Temperature can modify the interaction between the mild steel electrode and the acidic medium in the absence and the presence of inhibitors. To assess the influence of temperature on corrosion and corrosion inhibition processes, the weight loss measurements were carried out at 303–333 K temperature range. The results obtained indicated that corrosion rates increase with rise of temperature both in uninhibited and inhibited solutions. The dependence of corrosion rate on the temperature can be regarded as an Arrhenius-type process, the rate of which is given by [42]:

$$W_{\text{corr}} = A \exp\left(-\frac{E_a}{RT}\right) \quad (10)$$

where  $E_a$  is the apparent activation corrosion energy,  $R$  is the universal gas constant,  $A$  is the Arrhenius pre-exponential factor, and  $T$  is the absolute temperature. The Arrhenius plot is shown in Fig. 11 for mild steel in free acid solution and inhibited solution containing 5-HOT. Linear plots were obtained from the slope  $(-E_a/R)$ , activation energy ( $E_a$ ) values are deduced and listed in Table 6.

The temperature dependence of the inhibiting effect and the comparison of the values of the apparent activation energy of the corrosion process in the absence and presence of inhibitors can provide further evidence concerning the mechanism of the inhibiting action [43–45]. The decrease of the inhibitor efficiency with temperature rise, which refers to a higher value of  $E_a$ , when compared to that in an acid with no inhibitor, is interpreted as an indication for an electrostatic character of the inhibitor's adsorption. The lower value of  $E_a$  in an inhibited solution when compared to that of an uninhibited one shows that strong chemisorption bond between the inhibitor and the metal is highly probable [46]. Activation energy,  $E_a$  values in the table are higher

for inhibited solution (for the different concentration) than the uninhibited one, indicating a strong inhibitive action of the additives by increasing energy barrier for the corrosion process, emphasizing the electrostatic character of the inhibitor's adsorption on the mild steel surface (physisorption).

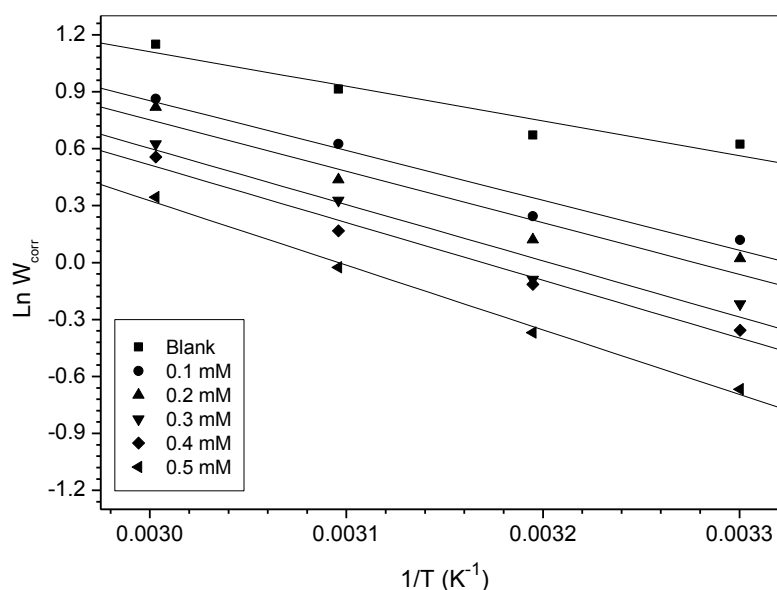


**Fig. 11.** Arrhenius plots for mild steel corrosion rate ( $W_{\text{corr}}$ ) in 1 M HCl in absence and in presence of different concentrations of 5-HOT.

**Table 6.** Activation parameters for mild steel corrosion in 1 M HCl in the absence and presence of 5-HOT.

Concentration (mM)	$E_a$ (kJ mol <sup>-1</sup> )	Ln A	$\Delta H_a$ (kJ mol <sup>-1</sup> )
Blank	22.60	6.59	20.31
0.1	21.84	8.73	19.20
0.2	22.56	8.89	19.92
0.3	24.62	9.48	21.98
0.4	25.25	9.62	22.61
0.5	28.29	10.53	25.65

### 3.3. XPS Surface analysis

In order to confirm the thermodynamic results and elucidate the nature of the organic thin film formed on the steel surface, the surface analysis was studied by XPS. For comparison purpose, the XPS spectra were obtained from the 5-HOT solid chemical, and the mild steel surface after 1 h of immersion in 1 M HCl containing 0.5 mM of 5-HOT (at this concentration, the highest inhibition efficiency was achieved as shown previously). The obtained XPS spectra (C 1s, N 1s, S 2p, O 1s, and Fe 2p core levels), given in Figs. 12 and 13, show complex forms, which were assigned to the corresponding species through a deconvolution fitting procedure. The binding energy (BE, eV) and the corresponding quantification (%) of each component are summarised in Table 7.

The C 1s spectrum for the 5-HOT solid chemical was deconvoluted into three peaks indicating three chemical forms of C atoms present on the oxadiazole derivative (Fig. 12a and Table 7). The largest peak can be attributed to contaminant hydrocarbons [47] and to the C–H, C–C, C=C aromatic bonds [13] with characteristic binding energy (BE) of 285.0 eV. The second peak may be ascribed to the C–O and C=N bonds in the oxadiazole ring and also to the carbon atom of the C–O bond in the phenol group located at 286.6 eV [48-49]. The last peak at a BE 288.8 eV may be attributed to C–O and C–S bonds [50]. However, C 1s spectrum for 5-HOT-treated mild steel displayed only two main peaks (Fig. 13a, Table 7). The deconvolution of this spectrum showed three components. Indeed, the first component at a BE ~ 285.0 eV is attributed to contaminant hydrocarbons and to the C–C, C=C and C–H aromatic bonds which the largest contribution. The second

component at 286.1 eV may be assigned to the carbon atoms bonded i) to nitrogen in C=N bonds in the oxadiazole ring, ii) to sulphur in C-S bond; and iii) to oxygen in the oxadiazole ring and in the phenol group. The last component at higher binding energy (located at approx. 288.8 eV) may be ascribed to the carbon atom of C-O bond and/or probably due to the C=N<sup>+</sup> [50], resulting from the protonation of the =N- structure in the oxadiazole ring.

The deconvolution of the N 1s spectrum of 5-HOT solid chemical might be fitted into two main components (Fig. 12b, Table 7). The first one at 400.4 eV was attributed to the unprotonated N atoms (=N- structure) in the oxadiazole ring [13,51]. The second component at higher binding energy (401.5 eV) is attributed to positively charged nitrogen, and could be related to protonated nitrogen atoms (=N<sup>+</sup>H-) in the oxadiazole ring [52]. Indeed, the molecular conformation of 5-HOT can yield intermolecular hydrogen bonding which leads to a positive polarization of the nitrogen atom and therefore an increased its binding energy [52]. Thus, the presence of the positively charged nitrogens (=N<sup>δ(+)</sup> structure) can be explained by hydrogen bonding between one hydrogen atom bonded to oxygen atom of the hydroxyl group and lone electron pair of a nitrogen atom of another oxadiazole molecule as illustrated in Fig. 14. The deconvolution of the N 1s spectrum of 5-HOT-treated mild steel revealed two components (Figs. 13b, Table 7). The most intense component, located at 400.2 eV, is assigned to =N- structure in the oxadiazole ring, while the less intense component (centered at 402.4 eV) can be ascribed to the positively charged nitrogen, and could be related to protonated nitrogen atoms (N<sup>+</sup>H-) in oxadiazole ring [53]. By comparing N 1s spectrum for the 5-HOT-treated steel with N 1s spectrum for the 5-HOT solid chemical, no significant change in peak position of =N- structure can be noticed. Moreover, the lower nitrogen content can be observed for the 5-HOT-treated steel. This behaviour suggests that 5-HOT molecules are not lying flat on the surface and that the N atoms in the 5-HOT molecules are not involved in the surface bonding with the steel substrate. This N 1s XPS result is consistent with the thermodynamic assumption that the 5-HOT was electrostatically adsorbed on the steel surface and the chemisorption has no substantial contribution.

The S 2p core-level of 5-HOT solid chemical is best resolved with at least two spin-orbit-split doublets (S 2p<sub>3/2</sub> and S 2p<sub>1/2</sub>, separated by 1.2 eV with an intensity ratio of  $I_{\text{peak S } 2p_{3/2}} / I_{\text{peak S } 2p_{1/2}} = 2$ ), with binding energy (BE) for S 2p<sub>3/2</sub> peak lying at about 162.8 eV (Fig. 13c, Table 7). This former can be assigned to the exocyclic sulphur atom (the thiol group (SH)) as mentioned previously [54]. After immersion in 1 M HCl, the S 2p spectrum of 5-HOT-treated steel, centered at 162.6 eV, can be attributed to the exocyclic sulphur atom (Fig. 13c). By comparing the S 2p spectra of 5-HOT-treated steel and 5-HOT solid chemical, one can notice the presence of sulphur on the steel surface but in low content. Moreover, the both S 2p spectra do not differ at the exocyclic S atom position, indicating that this sulphur is not involved in the 5-HOT bonding with the steel surface. In addition, the species containing an S-O bond are not present, as no additional peaks in the S 2p spectrum of 5-HOT-treated steel at a BE higher than 166 eV were detected [55]. Therefore, oxidation of the thiol group in the acidic medium did not occur.

The O 1s spectrum of 5-HOT solid chemical was fitted by three components (Fig. 13d, Table 7). The first two components at 531.8 and 533.4 eV may be assigned to singly bonded oxygen (-O-) in C-O in phenol group and O-H in hydroxyl group and also to O< structure in the oxadiazole moiety [56-57]. The last component at 535.0 eV can be attributed to oxygen of adsorbed water [58] and/or to oxygen of hydroxyl group, bonded to intermolecular hydrogen (Fig. 14). Indeed, the charging effect due to intermolecular hydrogen bonding could slightly move the peak position. The O 1s spectrum for mild steel surface after immersion in 1 M HCl solution containing 5-HOT could be fitted into three main peaks (Fig. 13d, Table 7). It's important noting that it is not possible to separate contributions of organic oxygen (O in C-O bond, OH...) since O 1s signal. The first peak, at approx. 530.3 eV, is ascribed to O<sup>2-</sup> and could be related to oxygen atoms bonded to Fe<sup>3+</sup> in the Fe<sub>2</sub>O<sub>3</sub> and/or Fe<sub>3</sub>O<sub>4</sub> oxides [59]. The second peak, observed at 531.7 eV, is attributed to OH<sup>-</sup>, can be associated to the presence of hydrous iron oxides, such as FeOOH [60]. Finally, the third peak at 532.9 eV may be assigned to oxygen of adsorbed water [61], which remained on the surface after drying the sample. These two last components may be also attributed to singly bonded oxygen (-O-) in phenol and hydroxyl groups, and to O< structure in the oxadiazole moiety which are present in 5-HOT.

The Fe 2p spectrum for mild steel surface treated with 5-HOT depicts a double peak profile located at a binding energy (BE) around 711 eV (Fe 2p<sub>3/2</sub>) and 725 eV (Fe 2p<sub>1/2</sub>) together with an associated ghost structure on the high energy side showing the subsequent oxidation of the steel surface. The deconvolution of the high resolution Fe 2p<sub>3/2</sub> XPS spectrum consists in four peaks (Fig. 13e, Table 7). The peak at lower binding energy (706.9 eV) is attributed to metallic iron as previously reported [62]. The peaks at 710.6 and 711.7 eV assigned to Fe<sup>3+</sup> [63], are in agreement with the presence of the iron oxide/hydroxide layer as detected in the O 1s

spectrum. The last peak at 713.5 eV was ascribed to the satellite of Fe(III) [64] and probably related to the presence of a small concentration of FeCl<sub>3</sub> on the steel surface due to the testing environment [65]. By comparing the Fe 2p<sub>3/2</sub> spectra for 5-HOT-treated steel (Fig. 13e) and untreated surface steel previously described [66], it's evident that the acidic medium containing 5-HOT induces a significant decrease in Fe<sup>0</sup> amount in favour of Fe<sup>3+</sup> species, indicating therefore that the oxide layer (iron oxide/hydroxide) thickness is increasing. Therefore, the addition of 5-HOT in the 1 M HCl solution promotes the formation of a stable and insoluble oxide layer (Fe<sub>2</sub>O<sub>3</sub>, FeOOH) and improves the corrosion resistance of mild steel in the corrosive environment.

On the basis of XPS analyses, the obtained results give evidence of electrostatic interactions between the 5-HOT inhibitor and mild steel surface (physisorption) and therefore corroborate the thermodynamic studies.

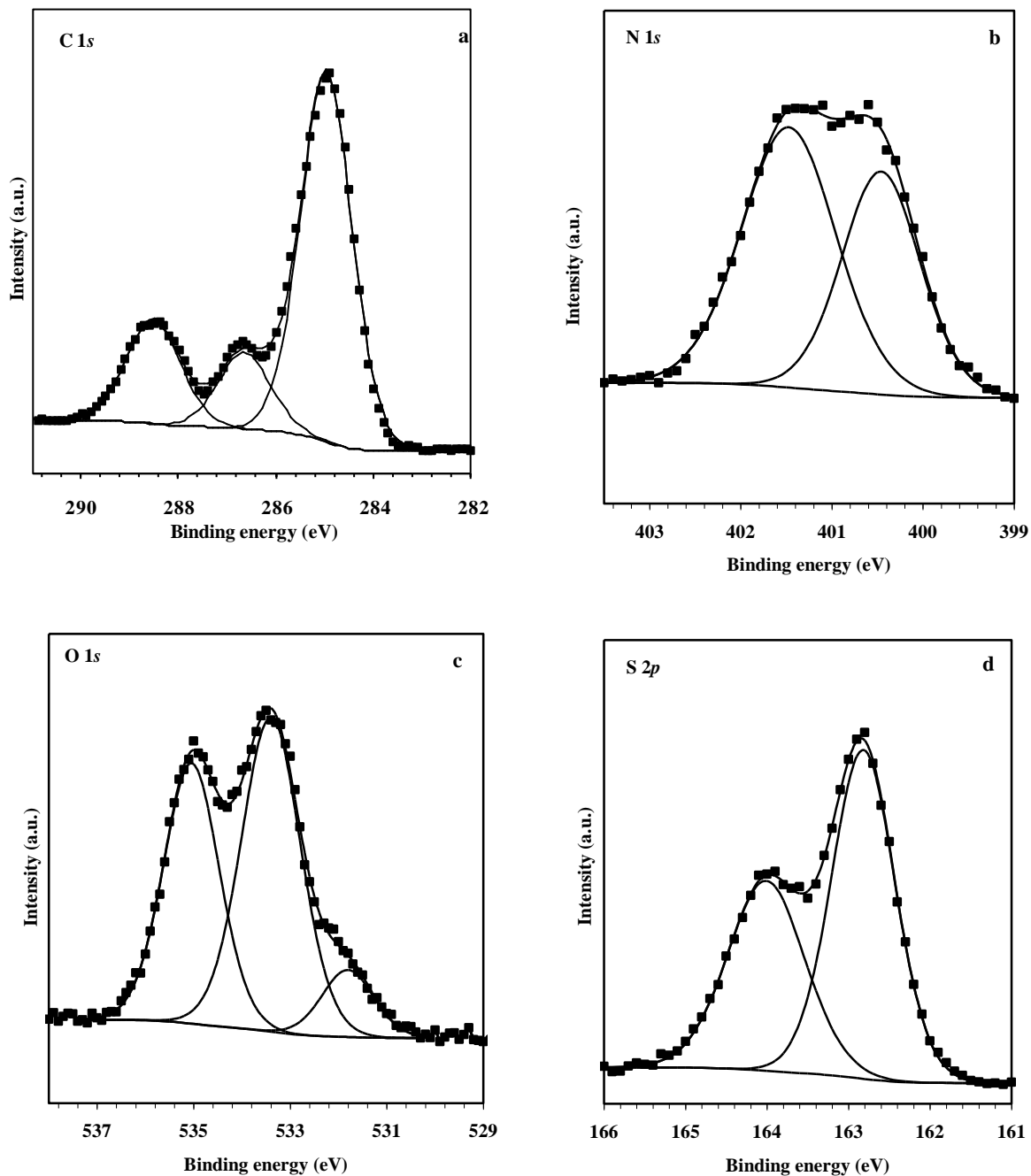


**Fig. 12.** The XPS deconvoluted profiles of a- C 1s, b- N 1s, c- O 1s, and d- S 2p for pure 5-HOT

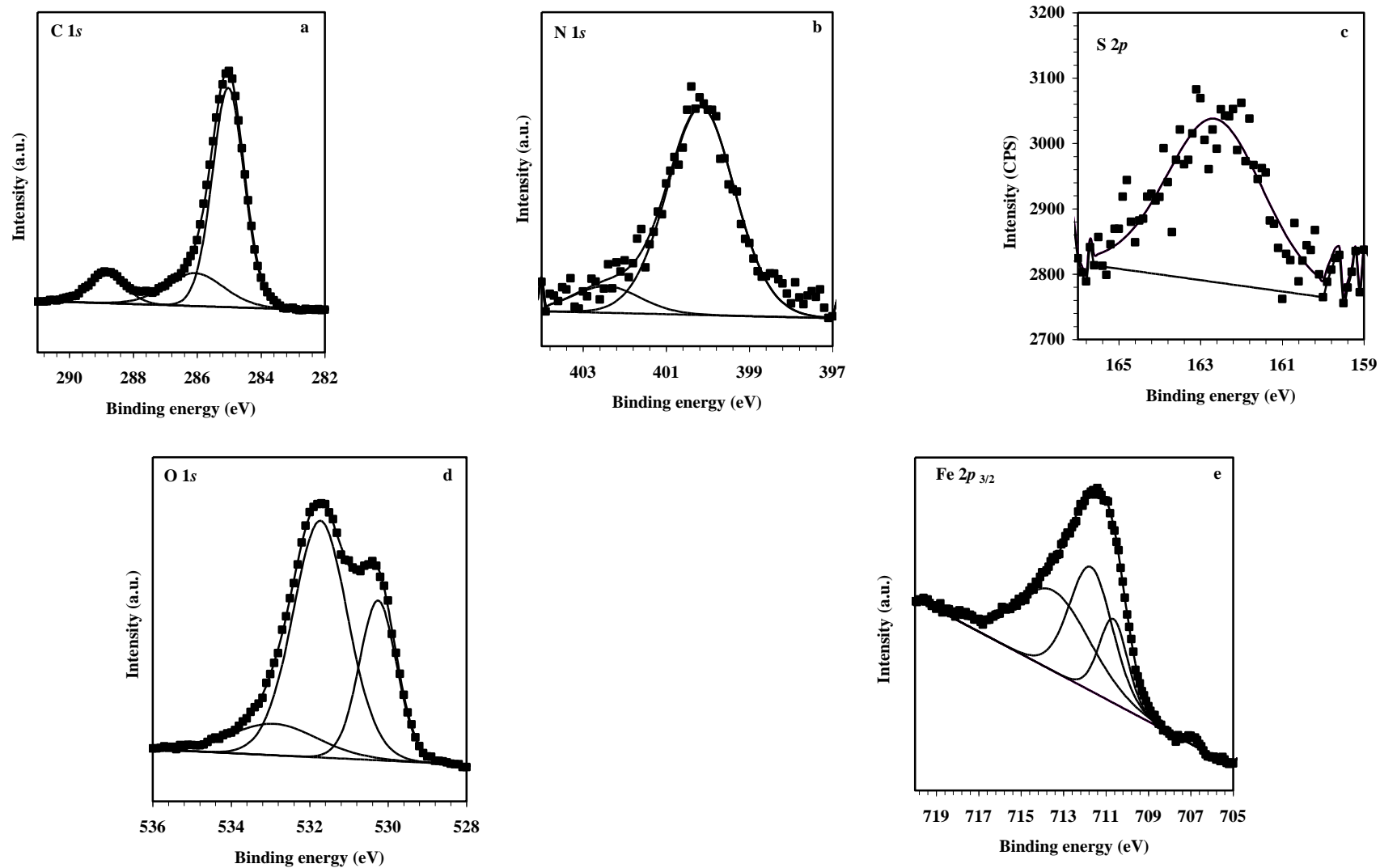


**Fig. 13.** The XPS deconvoluted profiles of a- C 1s, b- N 1s, c- S 2p, d- O 1s and e- Fe 2p<sub>3/2</sub> for 5-HOT treated mild steel.

**Table 7.** Binding energies (eV), relative intensity and their assignment for the major core lines observed in 5-HOT solid chemical and 5-HOT treated mild steel substrate spectra.

Substrate	C 1s		N 1s		S 2p		O 1s		Fe 2p <sub>3/2</sub>								
	BE / eV	Assignment	BE / eV	Assignment	BE / eV	Assignment	BE / eV	Assignment	BE / eV	Assignment							
5-HOT solid chemical	285.0 (66%)	C–H / C–C / C=C / Contaminant hydrocarbons	400.4 (42 %)	=N– structure	162.8 (59 %)	Thiol group (SH) S 2p <sub>3/2</sub>	531.8 (9 %)	O–C / O–H / O< (oxadiazole)	—	—							
		164.0 (41 %)			Thiol group (SH) S 2p <sub>1/2</sub>												
	286.6 (14 %)	C=N / C–O	401.5 (58 %)	=N <sup>δ(+)</sup> –	—	—	535.0 (51 %)	O–H <sup>δ(-)</sup> – / Adsorbed H <sub>2</sub> O	—	—							
	288.5 (14 %)	C–S / C–O	—	—	—	—	—	—	—	—							
5-HOT treated mild steel	285.0 (70%)	C–H / C–C / C=C / Contaminant hydrocarbons	400.2 (89 %)	=N– structure	160 - 166	Thiol group (SH)	530.3 (27 %)	Fe <sub>2</sub> O <sub>3</sub> / Fe <sub>3</sub> O <sub>4</sub>	706.9 (1 %)	F <sup>0</sup>							
		286.1 (19 %)			C=N / C–S	402.4 (11 %)					=N <sup>+</sup> –H	—	—	531.7 (60 %)	FeOOH / O–C / / O–H / O<	710.6 (17 %)	Fe <sub>2</sub> O <sub>3</sub> / Fe <sub>3</sub> O <sub>4</sub> / FeOOH
		288.8 (11%)			C–O / C=N <sup>+</sup>	—					—	—	—	532.9 (13 %)	Adsorbed H <sub>2</sub> O / O– / O<	713.5 (43 %)	Satellite of Fe(III) / FeCl <sub>3</sub>

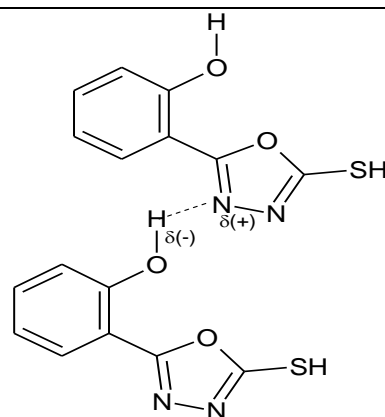


**Fig. 14.** Intermolecular hydrogen bonding of 5-HOT.

## Conclusions

5-(2-hydroxyphenyl)-1,3,4-oxadiazole-2-thiol (5-HOT) has been investigated as a corrosion inhibitor for mild steel in 1 M HCl medium at 303 K using weight loss and electrochemical techniques. The results showed that 5-HOT is effective inhibitor for mild steel corrosion in 1 M HCl solutions and its inhibition efficiency increases with the increase of 5-HOT concentration. Reasonably good agreement was observed between the obtained values from the weight loss, polarization, and electrochemical impedance techniques. Tafel polarization study showed that 5-HOT acts as mixed-type inhibitor. The EIS spectra were described well by the proposed structural model. The adsorption behavior of 1,3,4-oxadiazole derivative is consistent with Langmuir adsorption model at different temperatures. The calculated activation and the adsorptions thermodynamic parameters suggested that the corrosion inhibition mechanism of 5-HOT is mainly electrostatic-adsorption. XPS results supported the physisorption mode, and showed that the protective film is mainly composed by an iron oxide/hydroxide stable layer in which the 5-HOT molecules are incorporated, blocking therefore the active sites of the steel surface.

**Acknowledgments :** Prof. O. Benali extends his appreciation to Prof. M. Traisnel, Unité Matériaux et Transformations - École Nationale Supérieure de Chimie de Lille - France, for XPS analyses.

## References

1. Sastri V.S., *Corrosion Inhibitors-Principles and Applications*, Wiley, Chichester, England, 1998.
2. Said M. T., Ali S. A., Rahman S. U., *Anti-Corros. Method & Mater.* 50 (2003) 201–207.
3. Atia A., Saleh M. M., *J. Appl. Electrochem.*, 33 (2003)171–177.
4. Tamilselvi S., Rajeswari S., *Anti-Corros. Method & Mater.* 50 (2003) 223–231.
5. Keera S. T., *Anti-Corros. Method & Mater.* 50 (2003) 280-285.
6. Fouda A. S., Abdallah Y.M., Nabil D., *Inter. J. Innov. Res. Sci. Eng. Tech.*, 3 (2014)12965-12982.
7. Benali O., Larabi L., Tabti B., Harek Y., *Anti-Corros. Method & Mater.* 52 (2005) 280–285.
8. Ouici H.B., Benali O., Harek Y., Larabi L., Hammouti B., *Res. Chem. Intermed.* 39 (2013) 2777–2793.
9. Kumar P., Shetty A. N., *J. Mater. Environ. Sci.* 5 (2014) 873-886.
10. Pradeep Kumar C.B., Mohana K.N., *J. Chem. Pharm. Res.* 5 (2013) 289-305.
11. Tao Z., He W., Wang S., Zhang S., Zhou G., *Corros. Sci.* 60 (2012) 205-213.
12. Li W., Hu L., Tao Z., Tian H., Hou B., *Mater. Corros.* 62 (2011) 1042-1050.
13. Outirite M., Lagrenée M., Lebrini M., Traisnel M., Jama C., Vezin H., Bentiss F., *Electrochem. Acta* 55 (2010) 1670-1681.
14. Bouklah M., Hammouti B., Lagrenée M., Bentiss F., *Corros. Sci.* 48 (2006) 2831-2842.
15. Bentiss F., Traisnel M., Vezin H., Hildebrand H. F., Lagrenée M., *Corros. Sci.* 46 (2004)2781-2792.
16. Patel R.V., Patel P.K., Kumari P., Rajani D.P., Chikhalia K.H., *Europ. J. Med. Chem.* 53 (2012) 41-51.
17. Formagio A.S.N., Tonin L.T.D., Foglio M.A., *Bioorg. Medic. Chem.* 16 (2008) 9660–9667.
18. Murty M. S. R., Rao B.R., Katiki M.R., Nath L.R., Anto R.J., *Med. Chem. Res.* 22 (2013) 4980–4991.
19. Shirley D.A., *Phys. Rev. B* 5 (1972) 4709–4714.
20. Jayaperumal D., *Mater. Chem. Phys.* 119 (2010) 478–484.
21. Riggs Jr O.L., in *Corrosion Inhibitors*, ed. by C.C. Nathan (The National Association of Corrosion Engineers (NACE), Houston, 1973), pp. 2–27.
22. Anejjar A., Salghi R., Zarrouk A., Benali O., Zarrok H., Hammouti B., Al-Deyab S.S., Benchat N., Elaattiaoui A., *Int. J. Electrochem. Sci.* 8 (2013) 11512–11525.
23. Zhang S., Tao Z., Li W., Hou B., *Appl. Surf. Sci.* 255 (2009) 6757–6763.
24. Lorenz W.J., Mansfeld F., *Corros. Sci.* 21 (1981) 647–672.
25. Alagta A., Felhösi I., Bertoti I., Kálman E., *Corros. Sci.* 50 (2008) 1644–1649.
26. Reide F.M., Melo H.G., Costa I., *Electrochim. Acta* 51 (2006) 1780–1788.
27. Hsu C.H., Mansfeld F., *Corrosion* 57 (2001) 747-748.
28. Popova A., Christov M., Vasilev A., *Corros. Sci.* 49 (2007) 3290–3302.
29. Keddani M., Mattos O.R., Takenouti H., *J. Electrochem. Soc.* 128 (1981) 266–274.
30. Morales Roque J., Pandiyan T., Cruz J., García-Ochoa E., *Corros. Sci.* 50 (2008) 614–624.
31. Zarrouk A., Hammouti B., Lakhlifi T., Traisnel M., Vezin H., Bentiss F., *Corros. Sci.* 90 (2015) 572–584.
32. Zheludkevich M.L., Yasakau K.A., Poznyak S.K., Ferreira M.G.S., *Corros. Sci.* 47 (2005) 3368–3383.

33. Znini M., Majidi L., Bouyanzer A., Paolini J., Desjobert J.-M., Costa J., Hammouti B., *Arab. J. Chem.* 5 (2012) 467–474.
34. Yaro A. S., Abdulaaima D. A., *Iraqi J. Chem. Petrol. Eng.* 13 (2012) 1–9.
35. Khadom A. A., Yaro A. S., AlTaie A. S., Kadum A. A. H., *Port. Electrochem. Acta.* 27 (2009) 699–712.
36. Mall I. D., Srivastava V. C., Agarwal N. K., Mishra I. M., *Colloids Surf. A: Physicochem. Eng. Aspects* 264 (2005) 17–28.
37. Ostovari A., Hoseinieh S.M., Peikari M., Shadizadeh S.R., Hashemi S.J., *Corros. Sci.* 51 (2009) 1935–1949.
38. Durnie W., De Marco R., Kinsella B., Jefferson A., *J. Electrochem. Soc.* 146 (1999) 1751.
39. Moretti G., Guidi F., Fabris F., *Corros. Sci.* 76 (2013) 206–218.
40. Stoyanova A.E., Sokolova E.I., Raicheva S.N., *Corros. Sci.* 39 (1997) 1595.
41. Thomas J.M., Thomas W.J., in: *Introduction to the Principles of Heterogeneous Catalysis*, fifth ed., Academic Press, London, 1981, pp. 14–18.
42. Zarrouk A., Zarrok H., Salghi R., Hammouti B., Bentiss F., Tourir R., Bouachrine M., *J. Mater. Environ. Sci.* 4 (2) (2013) 177–192.
43. Ben Hmamou D., Aouad M. R., Salghi R., Zarrouk A., Assouag M., Benali O., Messali M., Zarrok H., Hammouti B., *J. Chem. Pharma. Res.*, 4 (2012) 3498-3504.
44. Ouici H. B., Benali O., Harek Y., Al-Deyab S.S., Larabi L., Hammouti B., *Int. J. Electrochem. Sci.*, 7 (2012) 2304 – 2319.
45. Salghi R., Anejjar A., Benali O., Al-Deyab S. S., Zarrouk A., Errami M., Hammouti B., Benchat N., *Int. J. Electrochem. Sci.* 9 (2014) 3087 – 3098.
46. El-Hajjaji F., Belkhemima R.A., Zerga B., Sfaira M., Taleb M., Ebn Touhami M., Hammouti B., Al-Deyab S.S., Eno Ebenso E., *Int. J. Electrochem. Sci.*, 9 (2014) 4721-4731.
47. Kannan A.G., Choudhury N.R., Dutta N.K., *Polymer* 48 (2007) 7078–7086.
48. Kelemen S.R., Afeworki M., Gorbaty M.L., *Energy Fuels* 16 (2002) 1450–1462.
49. Olivares O., Likhanova N.V., Gómez B., Navarrete J., Llanos-Serrano M.E., Arce E., Hallen J.M., *Appl. Surf. Sci.* 252 (2006) 2894–2909.
50. Watts J.F., Wolstenholme J., *An Introduction to surface analysis by XPS and AES*, John Wiley and Sons Inc., UK, 2003.
51. Kang E.T., Neoh K.G., Tan K.L., *Surf. Interface Anal.* 19 (1992) 33–37.
52. Bentiss F., Traisnel M., Gengembre L., Lagrenée M., *Appl. Surf. Sci.* 161 (2000) 194–202.
53. Schick G.A., Sun Z., *Langmuir* 10 (1994) 3105–3110.
54. Zhou J., Chen S., Zhang L., Feng Y., Zhai H., *J. Electroanal. Chem.* 612 (2008) 257–268.
55. Dietrich P.M., Horlacher T., Girard-Lauriault P.-L., Gross T., Lippitz A., Min H., Wirth T., Castelli R., Seeberger P.H., Unger W.E.S., *Langmuir* 27 (2011) 4808–4815.
56. Boyd R.D., Verran J., Hall K.E., Underhill C., Hibbert S., West R., *Appl. Surf. Sci.* 172 (2001) 135–143.
57. Kannan A.G., Choudhury N.R., Dutta N.K., *Polymer* 48 (2007) 7078–7086.
58. Finšgar M., *Corros. Sci.* 72 (2013) 90–98.
59. Bommersbach P., Alemany-Dumont C., Millet J.P., Normand B., *Electrochim. Acta* 51 (2005) 1076–1084.
60. Temesghen W., Sherwood P.M.A., *Anal. Bioanal. Chem.* 373 (2002) 601–608.
61. Babić-Samardžija K., Lupu C., Hackerman N., Barron A.R., Luttge A., *Langmuir* 21 (2005) 12187–12196.
62. Devaux R., Vouagner D., De Becdelievre A.M., Duret-Thual C., *Corros. Sci.* 36 (1994) 171–186.
63. Nakayamaand N., Obuchi A., *Corros. Sci.* 45 (2003) 2075–2092.
64. Galtayries A., Warocquier C. R., Nagel M.-D., Marcus P., *Surf. Interf. Anal.* 38 (2006) 186–190.
65. Sastri V.S., Elboujdaini M., Rown J.R., Perumareddi J.R., *Corrosion* 52 (1996) 447–452.
66. Lebrini M., Lagrenée M., Traisnel M., Gengembre L., Vezin H., Bentiss F., *Appl. Surf. Sci.* 253 (2007) 9267–9276.